



VICTORIA UNIVERSITY
MELBOURNE AUSTRALIA

Modeling of the electronic structure of semiconductor nanoparticles

This is the Published version of the following publication

Novozhilov, Vassili, Bodneva, Valeria L, Kurmangaleev, Kairat S, Lidskii, Boris V, Posvyanskii, Vladimir S and Trakhtenberg, Leonid I (2023) Modeling of the electronic structure of semiconductor nanoparticles. *Mathematics*, 11 (9). ISSN 2227-7390



The publisher's official version can be found at
<https://www.mdpi.com/2227-7390/11/9/2214>

Note that access to this version may require subscription.

Downloaded from VU Research Repository <https://vuir.vu.edu.au/46976/>

Article

Modeling of the Electronic Structure of Semiconductor Nanoparticles

Vasily B. Novozhilov ^{1,2,*}, Valeria L. Bodneva ², Kairat S. Kurmangaleev ², Boris V. Lidskii ², Vladimir S. Posvyanskii ² and Leonid I. Trakhtenberg ^{2,3}¹ Institute of Sustainable Industries and Liveable Cities, Victoria University, Melbourne, VIC 8001, Australia² N.N. Semenov Federal Research Centre of Chemical Physics, Russian Academy of Sciences, 4 Kosygina St., Building 1, Moscow 119991, Russia; vbodneva@yandex.ru (V.L.B.); f7033@mail.ru (K.S.K.); fishgoit@mail.ru (B.V.L.); vsposv@yandex.ru (V.S.P.); trakh@chph.ras.ru or litrakh@gmail.com (L.I.T.)³ Faculty of Chemistry, Lomonosov Moscow State University, Moscow 119991, Russia

* Correspondence: vasily.novozhilov@vu.edu.au

Abstract: This paper deals with the mathematical modeling of the electronic structure of semiconductor particles. Mathematically, the task is reduced to a joint solution of the problem of free energy minimization and the set of chemical kinetic equations describing the processes at the surface of a nanoparticle. The numerical modeling of the sensor effect is carried out in two steps. First, the number of charged oxygen atoms on the surface of the nanoparticle N_{O^-} is determined. This value is found by solving a system of nonlinear algebraic equations, where the unknowns are the stationary points of this system describing the processes on the surface of a nanoparticle. The specific form of such equations is determined by the type of nanoparticles and the mechanism of chemical reactions on the surface. The second step is to calculate the electron density inside the nanoparticle ($n_c(r)$), which gives the minimum free energy. Mathematically, this second step reduces to solving a boundary value problem for a nonlinear integro-differential equation. The calculation results are compared with experimental data on the sensor effect.

Keywords: sensors; conduction; calculus of variations; extremals; boundary value problem**MSC:** 49K21; 65M06; 82D80

Citation: Novozhilov, V.B.; Bodneva, V.L.; Kurmangaleev, K.S.; Lidskii, B.V.; Posvyanskii, V.S.; Trakhtenberg L.I. Modeling of the Electronic Structure of Semiconductor Nanoparticles. *Mathematics* **2023**, *11*, 2214. <https://doi.org/10.3390/math11092214>

Academic Editor: Dongfang Li

Received: 3 April 2023

Revised: 3 May 2023

Accepted: 5 May 2023

Published: 8 May 2023



Copyright: © 2023 by the authors. Licensee MDPI, Basel, Switzerland. This article is an open access article distributed under the terms and conditions of the Creative Commons Attribution (CC BY) license (<https://creativecommons.org/licenses/by/4.0/>).

1. Introduction

It is well known that processes involving metallic and semiconductor nanoparticles are at the base of many phenomena of both academic and practical interest. Their understanding is required for the investigation and utilization of conduction, sensor, photoelectric, catalytic, magnetic and other properties of nanocomposite materials [1–9]. It is clear that any investigation into the processes occurring in nanoparticles must focus on their charge structure.

The distribution of conduction electrons along the particle radius may be considered, due to their very high density, uniform for metallic nanoparticles. For semiconductor nanoparticles, however, the situation is drastically different. One should distinguish between semiconductor nanoparticles with low ($n_c \leq 10^{15} \text{ cm}^{-3}$) and high ($n_c \leq 10^{18}–10^{19} \text{ cm}^{-3}$) conduction electron densities. In both cases, the density is quite strongly temperature dependent.

Semiconductors with low conduction electron densities have less than one electron in the nanoparticle of the radius $R = 50 \text{ nm}$ (nanoparticles of SnO_2 and CeO_2 may serve as such an examples). It makes no sense, therefore, to speak about the electron structure of the nanoparticle in this case. In the case of the high conduction electron density (for example, In_2O_3 nanoparticles), the particle of the same size contains from 10^3 to 10^4 electrons [10,11]. It is then possible, with good reason, to consider the concept of the charge or electronic

structure of a nanoparticle. At such numbers, electrons form a definitive distribution along the radius, with part of them being pushed to the surface where they form a negatively charged surface layer (see, for example, [12,13]).

The choice of In_2O_3 nanoparticles as the object of study is due to several reasons. As is well known, nanostructured indium is widely used in microelectronics in the production of solar cells and phosphors, as well as high-temperature thermoelectric material [14]. The possibility of using indium in these areas is largely determined by the high concentration of conduction electrons, and especially by its concentration in the near-surface region of nanoparticles. Therefore, the elucidation of the distribution of electrons over the volume of nanoparticles is an extremely important task. Note also that a comparison of the theory with experimental data proposed in this article will be carried out for the sensor effect, for which the near-surface electron concentration is the determining factor.

The calculation of the electron distribution along the radius reduces to the problem of finding a minimum of the free energy (F). From the mathematical point of view, this is a problem of calculus of variations. Furthermore, conservation laws dictate some additional restrictions that must be imposed. Specifics of the functionals (F), considered in the present paper, are their rather complicated form. For this reason, the application of the theory developed in the present study to the functionals of the type (F) is a non-trivial task. The calculation of the variation of the functional is presented in a separate appendix of the paper. Conservation restrictions, upon the calculation of the variation, are being taken into account directly, without involving Lagrange multipliers. While canonical functionals give rise to a differential equation for the extremal, the corresponding equation in the present case is formally a nonlinear integro-differential.

This paper provides a detailed iterative solution process of the equation for the extremal. In order for discussion to be easily understandable, it is illustrated using the problem of calculation of a sensor effect. Sensors are devices that allow the detection of various substances, in particular gases, in different media. An example of such an application is a detection in the atmosphere of substances carrying fire and explosion hazards, as well as other gases having adverse effects on human health. The sensor effect manifests itself as a change in the conductance of the sensitive layer of a detector upon the action of gases that are being traced. As shown in the investigations [15,16], the conductance of a nano-structured sensitive layer depends on the electron distribution within the nanoparticle. The sensitivity of the detector is defined as a ratio of film conductance in the presence of hydrogen with the pressure P_{H_2} to conductance in its absence. This corresponds to the ratio of respective near-surface densities of conduction electrons in nanoparticles $\theta = \frac{n_c(R, P_{H_2})}{n_c(R, 0)}$, where R is the nanoparticle radius.

There is a significant number of studies devoted to the mechanism of the sensor effect; their detailed discussion is available in the review [17]. Equally, there are many studies discussing relevant calculation methodologies, for example, [18,19]. These papers consider the solution of Poisson's equation for spherical nanocrystal of a variable radius only. They consider neither the set of kinetic equations on the surface of the nanoparticle or the problem of minimization of free energy in the presence of restrictions. It is also worth while to mention the studies [15,20], which do consider, in some form, such formulations, but with a major emphasis on physics. Related essential techniques of the computational mathematics are not discussed in sufficient detail in these papers. The present paper aims at comprehensive discussion of mathematical problems, related to quantification of the sensor effect, such as minimization of free energy (i.e., calculation of variation), description of processes in negatively charged surface layer, and consideration of more complicated kinetics.

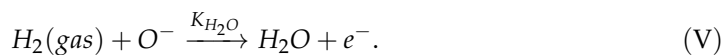
The present paper uses the following approach. The set of kinetic equations, describing various physico-chemical processes occurring on the surface of nanoparticle, is being developed. The solution of this set of equations determines the density of surface charges uniquely. Further, this set of equations is solved together with the problem of minimization

of free energy. The solution of the set of kinetic equations, corresponding to the processes on the surface of the nanoparticle, provides the boundary condition for the Poisson’s equation.

2. Mathematical Formulation

The formalisation of the problem under consideration is reduced to the solution of two mathematical problems. The first is the location of stationary points of the set of kinetic equations describing the physico-chemical processes on the surface of the nanoparticle of a given material, for example, In_2O_3 .

The chemical processes that take place on the surface of a nanoparticle are complicated and multistep, consisting of a large number of reactions. Let us consider only the most important reactions that take place on the surface of an indium oxide nanoparticle in the atmosphere:



Reaction (I) corresponds to the adsorption and desorption of molecular oxygen on the surface of a nanoparticle. Reaction (II) describes the dissociation of oxygen to atomic forms, as well as the reverse process. Reaction (III) corresponds to a conduction electron captured by an adsorbed atom of oxygen, and to the process of an electron returning to the volume of the nanoparticle [21]. Reaction (IV) describes the recombination of neutral and charged atoms of oxygen. The key role in the calculation of the sensor effect belongs to reaction (V). Here, as a result of the reaction between gaseous hydrogen and adsorbed oxygen ions, a molecule of water is formed, while the released electron migrates to the interior of the particle, thus increasing electron conductance. This change of electron conductance in the presence of hydrogen, compared to its value in the absence of hydrogen, is known as a sensor effect. The following set of kinetic equations represents the chemical reactions (I)–(V):

$$\begin{cases} \frac{dn_{O_2}}{dt} = K_{ad} \left(1 - \frac{n_O + n_{O_2}}{n_{O_2}^{lim}} \right) - K_{des}n_{O_2} + K_{rec}(n_O^2 - n_On_{O^-}) - K_{dis}n_{O_2} \left(1 - \frac{n_O + n_{O_2}}{n_{O_2}^{lim}} \right), \\ \frac{dn_O}{dt} = -2K_{rec}(n_O^2 - n_On_{O^-}) + 2K_{dis}n_{O_2} \left(1 - \frac{n_O + n_{O_2}}{n_{O_2}^{lim}} \right) - K_{O}^{des}(n_O - n_{O^-}) - K_{H_2O}\tilde{n}_{H_2}n_{O^-}, \\ \frac{dn_{O^-}}{dt} = (n_O - n_{O^-})(K_{cap} - K_{rec}n_{O^-}) - K_{ret}n_{O^-} - K_{H_2O}\tilde{n}_{H_2}n_{O^-}. \end{cases} \tag{1}$$

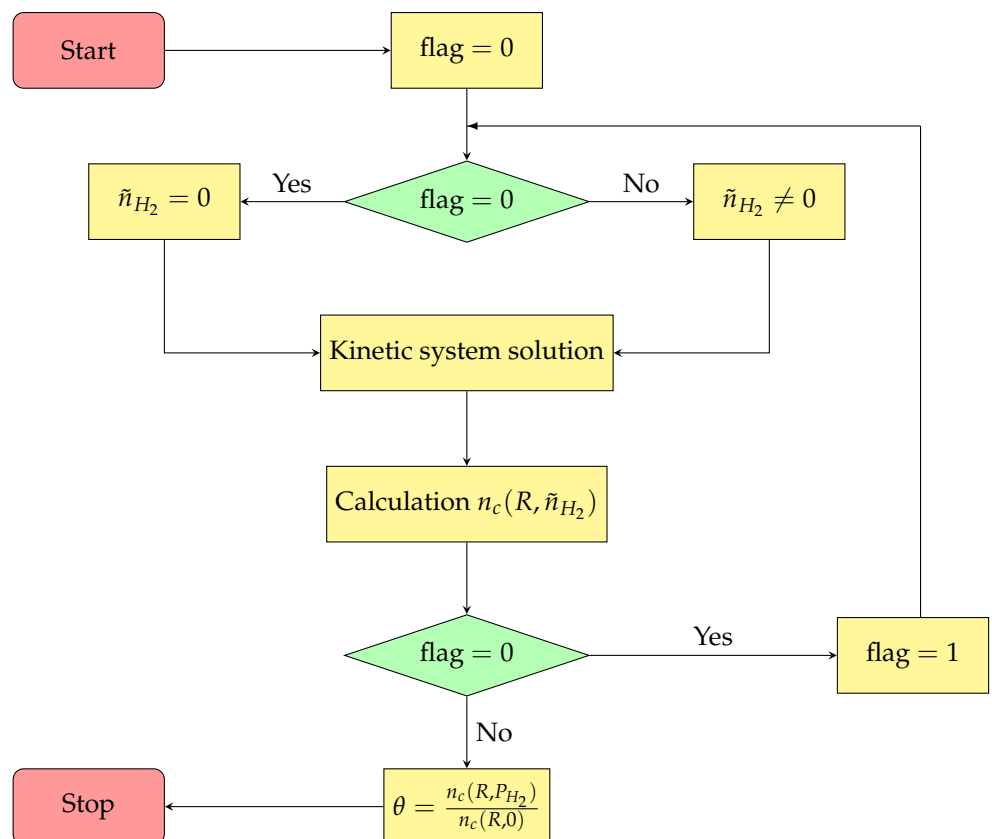
In the following analysis, the steady-state form of the set of Equation (1) is considered, since the sensor response time is much longer than the time constants of chemical reactions (I)–(V). Therefore, over the time comparable with the time constants, Equation (1) reaches the equilibrium. The reaction rate constants are considered as known functions of temperature (see Section 4). The unknowns are the surface density of the oxygen molecules n_{O_2} , the total surface density of all adsorbed forms of oxygen atoms (both neutral and negatively charged, O and O^-) n_O , and the surface density n_{O^-} of negative ions O^- . All of these variables have dimension $[cm^{-2}]$. The set of Equation (1) corresponds to the reaction scheme (I)–(V) and satisfies the laws of both the chemical kinetics and the theory of adsorption [22,23]. Various negatively charged forms of oxygen may adsorb on the surface

of the nanoparticle. In the range of sensor work temperatures ($T = 200\text{--}400\text{ }^\circ\text{C}$) O^- is the major form of adsorbed oxygen [24].

The set of Equation (1) is solved easily using, for example, the computational package Wolfram Mathematica. Note that the calculation of sensitivity to hydrogen requires the set of Equation (1) to be solved twice (see flowchart), the first time in the absence of hydrogen ($\tilde{n}_{\text{H}_2} = 0$), and the second time with its presence ($\tilde{n}_{\text{H}_2} \neq 0$).

For a different nanostructured system, for example, with a large family of different nanoparticles, this system will be of much higher order, and inevitably more complicated. It may have multiple solutions, including complex ones. In any case, though, this will be the set of nonlinear algebraic equations. Since n_{O} includes densities of both the neutral and the charged O atoms, the solution satisfying the condition $n_{\text{O}^-} < n_{\text{O}}$ must be singled out. In the case of an increased order, this set of steady-state equations is replaced by the set of nonsteady differential equations of chemical kinetics. Equilibrium points of the latter are solutions of the set of steady-state equations. Therefore, in the limit $t \rightarrow \infty$, the solution of set of the nonsteady equations approaches the required steady-state solution. It is known [25] that for the set of differential equations of chemical kinetics (in gaseous phase), the solution remains positive at any point in time if initial densities are non-negative. In particular, all the densities are positive at the equilibrium point. Moreover, such an equilibrium point is unique. As soon as the value n_{O^-} is found, the total charge on the nanoparticle's surface $N_{\text{O}^-} = 4\pi R^2 n_{\text{O}^-}$ (used at the second step of solution) may be determined, along with the value $N_{\text{O}} = 4\pi R^2 n_{\text{O}}$.

The following is the algorithm flowchart.



The second stage of the solution is much more demanding computationally. Here, it is necessary to find the electron density $n_c(r)$ and the density of positive ions $n_+(r)$ inside the nanoparticle, which provide the free energy minimum. At the same time, the balance between the total numbers of positive and negative charges N_+ and N_- must be carried out. Negative oxygen atoms, located on the surface of nanoparticles, have also to

be taken into account. All the variables (N_{O^-}, N_O, N_+, N_-) are dimensionless, i.e., just real numbers. From a mathematical point of view, this is the problem of calculus of variations with additional restriction [26].

Let us present free energy of the nanoparticle as a sum of free energies of the interacting charges [15,27,28].

$$F = F_1 + F_2 + F_3 + F_4. \tag{2}$$

Here F_1 is the free energy of conduction electrons [27]

$$F_1 = \int_0^R 4\pi r^2 F_{kin}(r) dr, \tag{3}$$

where density of free energy

$$F_{kin}(r) = -\frac{2\sqrt{2}(m^*)^{3/2}}{3\pi^2} \int_0^\infty \frac{\epsilon^{3/2} d\epsilon}{1 + \exp((\epsilon - \mu)/(kT))} + \mu n_c(r) \tag{4}$$

and

$$n_c = \frac{\sqrt{2}(m^*)^{3/2}}{\pi^2} \int_0^\infty \frac{\epsilon^{1/2} d\epsilon}{1 + \exp((\epsilon - \mu)/(kT))}. \tag{5}$$

Here, μ is the chemical potential, m^* is the effective mass of the electron, and $n_c(r)$ is the distribution of electron density over the radius inside of nanoparticles [27]. The Formula (4), as well as all subsequent formulae, are written in atomic units [29].

Let us write down the potential energy of the interaction between positive and negative charges of the nanoparticle [28].

$$F_2 = -(N_v - N_c - N_{O^-})\epsilon_v - kT \int_0^R 4\pi r^2 \left[n_v \ln \frac{n_v}{n_v - n_+(r)} + n_+(r) \ln \frac{n_v - n_+(r)}{n_+(r)} \right] dr, \tag{6}$$

where ϵ_v is the binding energy of electrons on donors [30] and $N_v = \frac{4\pi}{3} R^3 n_v$ is the donor density within nanoparticles.

Free energy of positively charged donors has the form [28]

$$F_3 = \frac{\epsilon_r}{2} \int_0^R r^2 \left(\frac{d\varphi}{dr} \right)^2 dr, \tag{7}$$

where φ is electrostatic potential within a semiconductor nanoparticle, ϵ_r is the relative dielectric permittivity, and the function φ satisfied the relationship

$$\frac{1}{r^2} \frac{\partial}{\partial r} \left(r^2 \frac{\partial \varphi}{\partial r} \right) = -\frac{4\pi}{\epsilon_r} (n_+ - n_c). \tag{8}$$

Formally, this relationship is not an equation since its left-hand side depends on the unknown function φ , while the right-hand side depends on the unknown functions μ and n_+ .

The last term in the expression (2) represents the free energy of negatively charged adsorbed ions of oxygen [15]:

$$F_4 = -N_{O^-} (\epsilon_0 + kT \ln 2) \left[N_O \ln \frac{N_O}{N_O - N_{O^-}} + N_{O^-} \ln \frac{N_O - N_{O^-}}{N_{O^-}} \right]. \tag{9}$$

Here ϵ_0 is the binding energy of an electron with the adsorbed atom of oxygen.

It is necessary to find the functions $n_c(r)$ and $n_+(r)$, which provide the minimum of free energy F . For this purpose, it is necessary to calculate the variation of the functional (2). Equating the variation to zero, we obtain relations that will be satisfied along the extremals (see Appendix A)

$$\mu = \varphi + C_1, \quad C_2 - C_1 = \varepsilon_v, \quad n_+ = \frac{n_v}{1 + \exp((\varphi + C_2)/kT)}. \tag{10}$$

C_1 is an arbitrary constant.

It follows from (10) that μ and n_+ on the extremals are functions of φ , and the electron density n_c is also a function of φ

$$n_c(\varphi) = \frac{\sqrt{2}(m^*)^{3/2}}{\pi^2} \int_0^\infty \frac{\varepsilon^{1/2} d\varepsilon}{1 + \exp((\varepsilon - \varphi - C_1)/(kT))} = -\frac{1}{\sqrt{2}} \left(\frac{m^*kT}{\pi} \right)^{3/2} Li_{3/2}(-e^m),$$

$$m = \frac{\varphi + C_1}{kT}. \tag{11}$$

Here, the polylogarithm special function $Li_s(z)$ is defined as an infinite power $Li_s(z) = \sum_{j=1}^\infty z^j / j^s$. The Wolfram Mathematica package calculates the function PolyLog[s, z] explicitly.

Positive charges are located within the internal region of the nanoparticle $r \in [0, R]$ only, and their number is

$$N_+ = 4\pi \int_0^R r^2 n_+(r) dr. \tag{12}$$

As for the negative particles (i.e., electrons), some of them can migrate to the surface of a nanoparticle and then be captured by adsorbed oxygen atoms. As a result of such a process, negatively charged oxygen ions O^- are being formed. The surface layer of the thickness d , containing N_{O^-} electrons (N_{O^-} is the number of electrons that have appeared on the surface) emerges. Therefore, the radius of the ball containing such electrons is $R + d$. Let us assume that electrons are distributed uniformly within the interval $r \in [R, R + d]$ and their total number may be written in the form

$$N_- = 4\pi \int_0^R r^2 n_c(r) dr + N_{O^-}. \tag{13}$$

Due to expressions (10) and (11), the relationship (8) becomes a sterling equation, depending on the parameter C_1 , for the unknown function φ . As a result, a boundary value problem for this function on the interval $r \in [0, R + d]$ is defined. It is formally an integro-differential (see expression (11)) Poisson's equation

$$\frac{1}{r^2} \frac{\partial}{\partial r} \left(r^2 \frac{\partial \varphi}{\partial r} \right) = \Phi(\varphi),$$

$$\Phi(\varphi(r)) = \begin{cases} -\frac{4\pi}{\varepsilon_r} (n_+(\varphi(r)) - n_c(\varphi(r))), & 0 < r < R, \\ \frac{4\pi}{\varepsilon_r} \bar{n}_c, & R < r < R + d, \quad \bar{n}_c = \frac{N_{O^-}}{V}, \end{cases} \tag{14}$$

with the boundary conditions at the ends of the interval

$$\frac{\partial \varphi}{\partial r} = 0, \text{ at } r = 0 \text{ and at } r = R + d. \tag{15}$$

Here, d is thickness of the layer with oxygen traps, $V = \frac{4\pi}{3}((R + d)^3 - R^3)$ is the volume of the spherical layer between R and $R + d$, and \bar{n}_c is the constant corresponding to uniform

distribution of anions within the layer. The boundary value problems (14) and (15) must be solved under the balance restriction

$$N_- = N_+. \tag{16}$$

As noted above, (Formulas (10) and (11)), the functions n_c, n_+ depend on the arbitrary constant C_1 . This constant is chosen in such a way that the balance restriction (16) is fulfilled.

Integrating Equation (14) over the interval $r \in [0, R]$, and taking into account restriction (16), we obtain

$$\frac{\partial \varphi}{\partial r} \Big|_{R-0} = -\frac{N_{O^-}}{R^2 \epsilon_r}. \tag{17}$$

Consider Equation (14) on the interval $r \in [R, R + d]$. It admits analytical solution. Moreover, the potential φ is defined up to an arbitrary constant. The solution that satisfies both the boundary condition (15) and the condition $\varphi(R + d) = 0$ is

$$\begin{aligned} \varphi(r) &= \frac{4\pi \bar{n}_c}{\epsilon_r} \left(\frac{r^2}{6} + \frac{(R + d)^3}{3r} - \frac{(R + d)^2}{2} \right), \\ \frac{\partial \varphi}{\partial r} \Big|_{R+0} &= -\frac{N_{O^-}}{R^2 \epsilon_r}. \end{aligned} \tag{18}$$

A comparison of expressions (17) and (18) shows that, provided fulfillment of the balance and adopted choice of \bar{n}_c , left and right derivatives at the point $r = R$ coincide. Thus, the second stage is being reduced to a solution of Equation (14) within the nanoparticle $r \in [0, R]$ only, but with the boundary conditions

$$\frac{\partial \varphi}{\partial r}(0) = 0, \quad \varphi(R) = \frac{4\pi \bar{n}_c}{\epsilon_r} \left(\frac{R^2}{6} + \frac{(R + d)^3}{3R} - \frac{(R + d)^2}{2} \right). \tag{19}$$

In this case, continuity of the solution of Equation (14) and its derivatives at $r = R$ (i.e., at the point of discontinuity of the right-hand side $\Phi(\varphi)$) would be warranted.

3. Numerical Method

The boundary value problem for Equation (14) with the conditions (19) on the interval $r \in [0, R]$ was solved numerically by the method of time development [31]. According to this method, the solution of the steady-state equation is obtained as the limit at $t \rightarrow \infty$ of the solution of the nonsteady equation

$$\frac{\partial \varphi}{\partial t} = \frac{1}{r^2} \frac{\partial}{\partial r} \left(r^2 \frac{\partial \varphi}{\partial r} \right) - \Phi(\varphi). \tag{20}$$

Here t is a false time, formally introduced into the problem. The method of time development may be interpreted as an iteration process. The initial distribution at $t = 0$ serves as a zeroth-order approximation. The solution at the next time layer corresponds to current iteration. The main advantage of the method of time development is a very weak dependence of the convergence on the initial distribution.

Equation (20) was solved by the finite difference method, using the following implicit scheme:

$$\begin{aligned} \frac{\varphi_i^{n+1} - \varphi_i^n}{\tau_n} &= \frac{2}{r_i^2 (h_{i+1} + h_i)} \left[r_{i+1/2}^2 \frac{\varphi_{i+1}^{n+1} - \varphi_i^{n+1}}{h_{i+1}} - r_{i-1/2}^2 \frac{\varphi_i^{n+1} - \varphi_{i-1}^{n+1}}{h_i} \right] - \\ &- \Phi(\varphi_i^s) - \Phi'(\varphi_i^s)(\varphi_i^{n+1} - \varphi_i^s). \end{aligned} \tag{21}$$

The integrals on the right side of $\Phi(\varphi)$ were calculated using the polylogarithm function, as mentioned earlier. Tables of the required functions $Li_{3/2}(z)$, $Li_{1/2}(z)$ in a wide range of the argument z were created in advance using the Wolfram Mathematica package. Interpolation within these tables was then used to calculate the values of the integrals.

As the function $\Phi(\varphi)$ is nonlinear, its preliminary linearization was necessary. The derivative Φ'_φ was calculated using the relationship $\frac{\partial Li_n(-e^m)}{\partial m} = Li_{n-1}(-e^m)$. Due to non-linearity of the problem, internal iterations (where s is iteration number) were performed at each time layer. The solution from the previous layer was used as the first internal iteration. The set of linear equations, emerging at the upper layer, was solved by the Thomas algorithm. A variable time step was used. In the case of quick (in less than three) internal iterations convergence, the time step was doubled. Naturally, the convergence rate increased upon approaching the steady-state solution, and so did the time step τ_n . The solution process stopped once the time step became very large ($\tau_n \gg 1$). The implicit finite difference scheme (21) is stable for any relation between time and spatial discretizations. Due to this fact, iterations were performed with a larger time step upon approaching the steady-state solution. It should be emphasized that fulfillment of the balance condition (16), which is equivalent to the adjustment of the constant C_1 in (10), requires the steady-state solution of Equation (21) to be obtained repetitively.

The described methodology was implemented into the in-house computational code developed at the N.N. Semenov Federal Research Centre of Chemical Physics, Russian Academy of Sciences. The code was written in C++ using Microsoft Visual Studio 2008.

4. Results and Comparison with the Experimental Data

The free energy minimization method and consideration of the chemical system on the surface of a nanoparticle have been used extensively for comparison between the theory and experiment by investigating the infrared radiation absorption and sensor effect (see, for example, [15,20]). The results for the case of the sensing layer consisting solely of the oxide In_2O_3 nanoparticles are presented below. The set of Equation (1) corresponds exactly to this case. All the calculations, with adjustment of parameters, were performed using Atomic System Units (ASU) [29]. The relationship between the main units in the ASU and the SI system is given below (Table 1).

Table 1. Major atomic units.

Mass unit in ASU	m_e	9.109×10^{-31} kg
Length unit in ASU	a_0	5.292×10^{-11} m
Time unit in ASU	t_h	2.419×10^{-17} s
Energy unit in ASU	E_h	4.360×10^{-18} J

Tables 2 and 3 provide the expressions for reaction rate constants as functions of temperature. The values of the parameters are given in Table 4. See also the short discussion at the end of the Section 4.

Table 2. Rate constants of surface reactions.

Parameter	Meaning	Value
$K_{dis} [t_h^{-1}]$	dissociation constant of adsorbed molecules O_2	$\nu_{O-O} \exp(-\frac{\epsilon_{dis}}{kT})$
$K_{rec} [a_0^2 t_h^{-1}]$	recombination constant of adsorbed atoms O	$a_O^2 \nu_O \exp(-\frac{\epsilon_a^O}{kT})$
$K_{ad} [a_0^{-2} t_h^{-1}]$	adsorption constant of molecules O_2	$\frac{1}{4} \tilde{n}_{O_2} \sqrt{\frac{3kT}{m_{O_2}}} \alpha_{O_2}(T)$

Table 2. Cont.

Parameter	Meaning	Value
$K_{des} [t_h^{-1}]$	desorption constant of molecules O_2	$\nu_{O_2} \exp(-\frac{\epsilon_{des}}{kT})$
$K_O^{des} [t_h^{-1}]$	desorption constant of atoms O	$\nu_O^{des} \exp(-\frac{\epsilon_{des}^O}{kT})$
$K_{ret} [t_h^{-1}]$	electron return constant into nanoparticle volume	$\nu_{ret} \exp(-\frac{\epsilon_{ret}}{kT})$

Table 3. Rate constants of surface reactions, determined by the experiment.

Parameter	Meaning	Value
$K_{cap} [t_h^{-1}]$	electron capture constant by oxygen atom	$1.25 \times 10^{-17} + 3.07 \times 10^{-19} e^{\frac{T-383.94}{96.07}}$
$K_{H_2O} [a_0^3 t_h^{-1}]$	reaction rate constant of hydrogen-oxygen reaction	$7.92 \times 10^{-11} T e^{-\frac{486.34}{T}}$

The parameters in Table 4 correspond to the rate constants of the surface reactions included in system 1 (see also reactions (I)–(V)). Therefore, they were selected for the fitting procedure. Obtaining a fitting procedure with physical reasonable values of parameters allows us to consider the constructed model as adequate. So, the following values of parameters were used in calculations.

Table 4. Data providing best agreement with experiment.

Parameter	Value	Dimension	References
ϵ_{dis}	4.32×10^{-2}	E_h	
ϵ_a^O	6.6×10^{-2}	E_h	
ϵ_{des}	2.8×10^{-2}	E_h	[32]
ϵ_{des}^O	2.9×10^{-2}	E_h	
ϵ_{ret}	2.3×10^{-2}	E_h	
ϵ_v	7.35×10^{-3}	E_h	[33,34]
ϵ_O	10^{-3}	E_h	
ν_{O-O}	2.4×10^{-4}	t_h^{-1}	[35]
ν_{O_2}	2.4×10^{-5}	t_h^{-1}	[35]
ν_O^{des}	7.5×10^{-5}	t_h^{-1}	[35]
ν_O	2.4×10^{-4}	t_h^{-1}	[35]
ν_{ret}	2.36×10^{-13}	t_h^{-1}	
n_v	2.16×10^{-6}	a_0^{-3}	[11]
\tilde{n}_{O_2}	1.15×10^{-6}	a_0^{-3}	[36]
\tilde{n}_{H_2}	4×10^{-9}	a_0^{-3}	
$n_{O_2}^{lim}$	1.12×10^{-2}	a_0^{-2}	
a_O	2	a_0^2	
ϵ_r	5	dimensionless	[37]
m_{O_2}	5.9×10^4	m_e	
m^*	2	m_e	
R	700	a_0	
$\alpha_{O_2}(T)$	$3.8 \times T^{1.69} e^{-\frac{11664.3}{T}}$	dimensionless	

Figure 1 demonstrates good performance of the developed model for interpretation of experimental data on the dependence of the sensor effect (θ) on temperature (T). Details of the experiment are available in [38]. The resistance of the film of In_2O_3 , laid over a dielectric substrate, was measured for the two cases: (i) in the stream of air, and (ii) in the stream of air with addition of H_2 . The sensor effect is a ratio of these resistances. The measurements were conducted at various temperatures. The results were verified using five different samples of the film. The maximum error in resistance measurement was 2.5%.

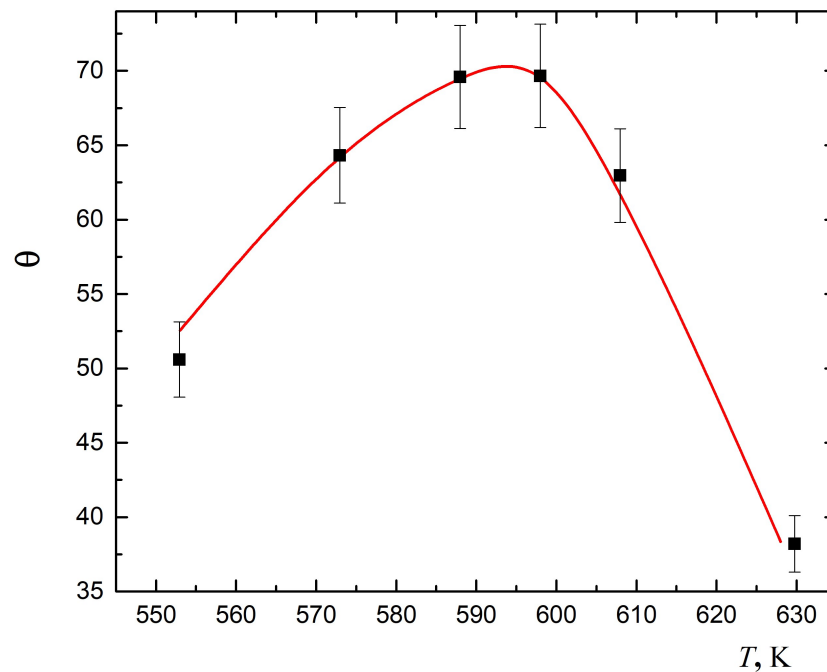


Figure 1. The temperature dependence of the sensor effect for In_2O_3 system at 2% hydrogen in the air. The dots represent the experimental data [38]. The curve is the calculation result (fitting).

Numerical experiments were conducted in order to achieve the best agreement with the experimental data. The values of the parameters delivering the best agreement are reported in Table 4. These values have been partly extracted from existing publications, in particular, the measured values of the following: dielectric permittivity of nanoparticle material ϵ_r , energy of donor level in the indium oxide ϵ_v , density of donors n_v in the volume of a semiconductor nanoparticle, volume density of oxygen in the air \tilde{n}_{O_2} , frequency of stretching vibrations of atoms in adsorbed oxygen molecule ν_{O-O} (of the order of 10^{12} – 10^{13} s^{-1}), and the energy required to tear off the molecule of oxygen from the surface of indium oxide ϵ_{des} . Constants of the rate of the electron capture by the oxygen atom K_{cap} and the reaction of hydrogen with adsorbed oxygen ions K_{H_2O} were estimated directly from the experiments on kinetics of resistance variation upon the injection of hydrogen and oxygen. The rest of the parameter values were adopted based on the best agreement with the experimental data on the sensor effect to hydrogen.

The developed technique for describing processes occurring in simple nanostructured materials also works in more complex cases. So, for illustration, in Figure 2, the recently obtained results of comparing the theory with experimental data for the mixed system CeO_2 - In_2O_3 [39] is presented. The fitting procedure is slightly more complicated; along with processes (I)–(V), the chemical reactions on the surface of CeO_2 nanoclusters and the transfer of reaction products to In_2O_3 nanoparticles should be taken into account. Accordingly, the system of kinetic equations will also change, but there are no fundamental innovations.

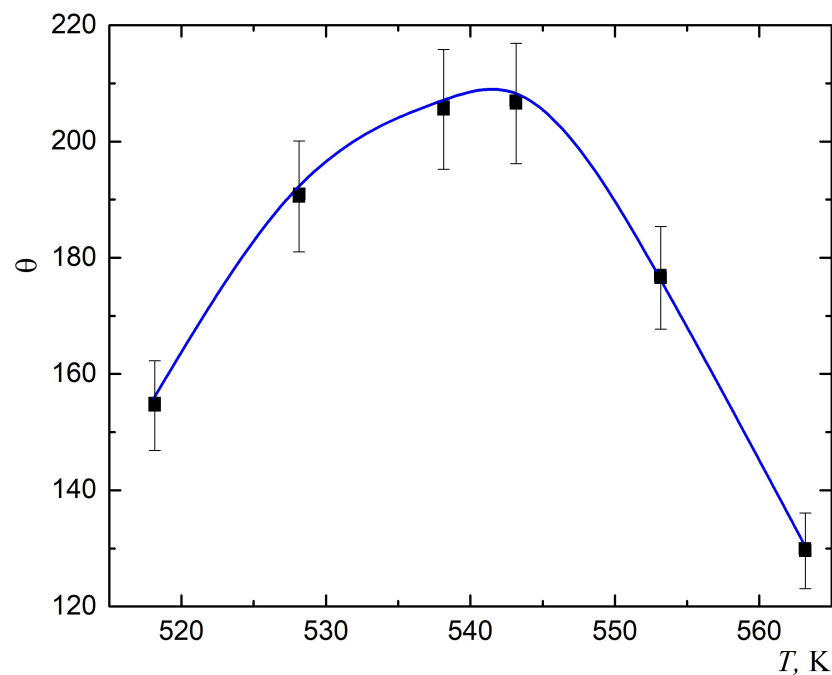


Figure 2. The temperature dependence of the sensor effect for the mixed system $CeO_2-In_2O_3$ at 2% hydrogen in the air. The dots represent the experimental data [39]. The curve is the calculation result (fitting).

5. Conclusions

The present study demonstrates advances in mathematical modeling of physico-chemical processes using the example of the sensor effect. A methodology and an algorithm for such a modeling have been developed. They consist of the following steps. First, appropriate equations describing kinetics of the given process are chosen. Further, these equations are being solved to obtain expressions for n_{O_2}, n_O, n_{O^-} , which are required for the calculation of the distribution function $n_c(r)$ of elections along the radius of the nanoparticle. Obviously, solutions of the set of Equation (1) are different depending on the presence or absence of hydrogen. In order to calculate the function $n_c(r)$, the problem of the minimization of free energy is considered. The latter problem reduces to a boundary value problem for the Poisson's equation. The boundary condition at the right boundary of the nanoparticle was set using the earlier found value n_{O^-} . The steady-state Poisson's equation was solved by the method of time development.

Based on the proposed algorithm, an in-house computer code was developed.

A comparison between the calculations and experimental data was performed using the examples of sensitivity of the layer based on In_2O_3 and the mixed system $CeO_2-In_2O_3$ to hydrogen.

The application of the developed methodology and computational code is not restricted to the calculation of the distribution of the charge in spherical semiconductor nanoparticles in a vacuum in the presence of various gases. They can also be used for the solutions of other problems, such as the quantification of the influence of external electrostatic fields on distributions of charge and electrical fields in nanosystems of various shapes such as cone-like, spherical, and rectangular shapes.

Author Contributions: Conceptualization, V.B.N., V.L.B., K.S.K., B.V.L., V.S.P. and L.I.T.; Methodology, V.B.N., V.L.B., K.S.K., B.V.L., V.S.P. and L.I.T.; Investigation, V.B.N., V.L.B., K.S.K., B.V.L., V.S.P. and L.I.T.; Writing—original draft, V.B.N., V.L.B., K.S.K., B.V.L., V.S.P. and L.I.T. All the authors contributed equally to the study. All authors have read and agreed to the published version of the manuscript.

Funding: The work was supported by a subsidy from the Ministry of Education and Science of the Russian Federation for N.N. Semenov Federal Research Centre of Chemical Physics, Russian Academy of Sciences, within the framework of the State Assignment No. 122040500071-0.

Data Availability Statement: The data are available from the authors upon request.

Conflicts of Interest: The authors declare no conflicts of interest.

Appendix A

Variation of the functional F , under the balance constraints (16), is calculated as follows

$$\begin{aligned} \delta F_1 &= 4\pi \int_0^R r^2 \frac{\partial F_{kin}}{\partial n_c} \delta n_c dr. \\ \frac{\partial F_{kin}}{\partial \mu} &= -\frac{2\sqrt{2}(m^*)^{3/2}}{3\pi^2 kT} \int_0^\infty \frac{\varepsilon^{3/2} \exp((\varepsilon - \mu)/(kT)) d\varepsilon}{(1 + \exp((\varepsilon - \mu)/(kT)))^2} + n_c(r) + \mu \frac{\partial n_c}{\partial \mu} = \text{(in parts)} \\ &- \frac{\sqrt{2}(m^*)^{3/2}}{\pi^2} \int_0^\infty \frac{\varepsilon^{1/2} d\varepsilon}{1 + \exp((\varepsilon - \mu)/(kT))} + n_c(r) + \mu \frac{\partial n_c}{\partial \mu} = \mu \frac{\partial n_c}{\partial \mu}. \tag{A1} \\ \frac{\partial F_{kin}}{\partial n_c} &= \frac{\partial F_{kin}}{\partial \mu} \frac{\partial \mu}{\partial n_c} = \mu. \\ \delta F_1 &= 4\pi \int_0^R r^2 \mu \delta n_c dr. \end{aligned}$$

Let us assume, for the time being, that

$$\int_0^R r^2 \delta n_c dr = \int_0^R r^2 \delta n_+ dr = 0. \tag{A2}$$

then

$$\begin{aligned} \delta F_2 &= -kT \int_0^R 4\pi r^2 \frac{\partial}{\partial n_+} \left[n_v \ln \frac{n_v}{n_v - n_+(r)} + n_+(r) \ln \frac{n_v - n_+(r)}{n_+(r)} \right] \delta n_+ dr = \\ &-kT \int_0^R 4\pi r^2 \ln \frac{n_v - n_+(r)}{n_+(r)} \delta n_+ dr. \tag{A3} \end{aligned}$$

$$\delta n = \delta n_+ - \delta n_c.$$

$$\frac{\partial \varphi}{\partial r} = -\frac{4\pi}{\chi r^2} \int_0^r n(\alpha) \alpha^2 d\alpha; \text{ (assume that, } \varphi'_r(0) = 0).$$

$$F_3 = \frac{8\pi^2}{\chi} \int_0^R \frac{1}{r^2} \left(\int_0^r n(\alpha) \alpha^2 d\alpha \right)^2 dr. \tag{A4}$$

$$\begin{aligned} \delta F_3 &= \frac{16\pi^2}{\chi} \int_0^R \frac{1}{r^2} \left(\int_0^r \delta n(\alpha) \alpha^2 d\alpha \right) \left(\int_0^r n(\gamma) \gamma^2 d\gamma \right) dr = \\ &-4\pi \int_0^R \left(\int_0^r \delta n(\alpha) \alpha^2 d\alpha \right) \frac{\partial \varphi}{\partial r} dr = -4\pi \varphi \left(\int_0^R \delta n(\alpha) \alpha^2 d\alpha \right)_0^R + 4\pi \int_0^R r^2 \varphi(r) \delta n(r) dr. \end{aligned}$$

Since $\int_0^r \delta n(r) r^2 dr = 0$ (full charge), then

$$\delta F_3 = 4\pi \int_0^R r^2 \varphi(r) (\delta n_+ - \delta n_c) dr. \quad (\text{A5})$$

Finally,

$$\delta F = 4\pi \int_0^R r^2 (\mu - \varphi) \delta n_c dr + 4\pi \int_0^R r^2 (\varphi - kT \ln \frac{n_v - n_+}{n_+}) \delta n_+ dr. \quad (\text{A6})$$

Therefore, we obtain the relationships

$$\begin{aligned} \mu &= \varphi + C_1. \\ \varphi - kT \ln \frac{n_v - n_+}{n_+} &= -C_2. \\ n_+ &= \frac{n_v}{1 + \exp((\varphi + C_2)/kT)}. \end{aligned} \quad (\text{A7})$$

If once assumes that $\int_0^r \delta n_+(r) r^2 dr \neq 0$, but $\int_0^r \delta n(r) r^2 dr = 0$ (balance condition is fulfilled), then

$$\begin{aligned} \delta F_2 &= \varepsilon_v 4\pi \int_0^r \delta n_c(r) r^2 dr - kT \int_0^R 4\pi r^2 \ln \frac{n_v - n_+(r)}{n_+(r)} \delta n_+ dr. \\ \delta F &= 4\pi \int_0^r (\varepsilon_v + C_1 - C_2) \delta n_c r^2 dr. \end{aligned} \quad (\text{A8})$$

From here, we obtain

$$C_2 - C_1 = \varepsilon_v. \quad (\text{A9})$$

References

- Nicolais, L.; Carotenuto, G. *Metal/Polymer Nanocomposites*; John Wiley and Sons: New York, NY, USA, 2005.
- Trakhtenberg, L.I.; Lin, S.H.; Ilegbusi, O.J. *Physico-Chemical Phenomena in Thin Films and at Solid Surfaces*; Elsevier Inc.: Amsterdam, The Netherlands, 2007.
- Achermann, M. Exciton-Plasmon Interactions in Metal-Semiconductor Nanostructures. *J. Phys. Chem. Lett.* **2010**, *1*, 2837–2843. [[CrossRef](#)]
- Garcia, G.; Buonsanti, R.; Runnerstrom, E.L.; Mendelsberg, R.J.; Llordes, A.; Anders, A.; Richardson, T.J.; Milliron, D.J. Dynamically Modulating the Surface Plasmon Resonance of Doped Semiconductor Nanocrystals. *Nano Lett.* **2011**, *11*, 4415–4420. [[CrossRef](#)] [[PubMed](#)]
- Boulaï, E.; Lachaine, R.; Hatef, A.; Meunier, M. Plasmonics for Pulsed-Laser Cell Nanosurgery: Fundamentals and applications. *J. Photochem. Photobiol. C* **2013**, *17*, 26–49. [[CrossRef](#)]
- Faucheaux, J.A.; Stanton, A.L.D.; Jain, P.K. Plasmon Resonances of Semiconductor Nanocrystals: Physical Principles and New Opportunities. *J. Phys. Chem. Lett.* **2014**, *5*, 976–985. [[CrossRef](#)] [[PubMed](#)]
- Schröfel, A.; Kratošová, G.; Safark, I.; Šafaříková, M.; Raška, I.; Shor, L.M. Applications of Biosynthesized Metallic Nanoparticles—A Review. *Acta Biomater.* **2014**, *10*, 4023–4042. [[CrossRef](#)] [[PubMed](#)]
- Granitzer, P.; Rumpf, K. *Nanostructured Semiconductors—From Basic Research to Applications*; Pan Stanford Publishing Ltd.: Singapore, 2014.
- Chen, T.; Liu, Y. *Semiconductor Nanocrystals and Metal Nanoparticles: Physical Properties and Device Applications*; CRC Press Taylor and Francis Group: Boca Raton, FL, USA, 2016.
- Jimenez, L.C.; Mendez, H.A.; Paez, B.A.; Ramirez, M.E.; Rodriguez, H. Production and Characterization of Indium Oxide and Indium Nitride. *Braz. J. Phys.* **2006**, *36*, 1017–1020. [[CrossRef](#)]

11. Prathap, P.; Gowri, D.G.; Subbaiah, Y.P.V.; Ramakrishna, R.K.T.; Ganesan, V. Growth and Characterization of Indium Oxide Films. *Curr. Appl. Phys.* **2008**, *8*, 120–127. [[CrossRef](#)]
12. Barsan, N.; Weimar, U. Conduction Model of Metal Oxide Gas Sensors. *J. Electroceram.* **2001**, *7*, 143–167. [[CrossRef](#)]
13. Yamazoe, N.; Shimano, K. Theoretical Approach to the Gas Response of Oxide Semiconductor Film Devices under Control of Gas Diffusion and Reaction Effects. *Sens. Actuators B* **2011**, *154*, 277–282. [[CrossRef](#)]
14. Lewis, B.G.; Paine, D.C. Applications and Processing of Transparent Conducting Oxides. *MRS Bull.* **2000**, *25*, 22–27. [[CrossRef](#)]
15. Bodneva, V.L.; Ilegbusi, O.J.; Kozhushner, M.A.; Kurmangaleev, K.S.; Posvyanskii, V.S.; Trakhtenberg, L.I. Modeling of Sensor Properties for Reducing Gases and Charge Distribution in Nanostructured Oxides: A Comparison of Theory with Experimental Data. *Sens. Actuators B Chem.* **2019**, *287*, 218–224. [[CrossRef](#)]
16. Kurmangaleev, K.S.; Ikim, M.I.; Kozhushner, M.A.; Trakhtenberg, L.I. Electron Distribution and Electrical Resistance in Nanostructured Mixed Oxides $CeO_2-In_2O_3$. *Appl. Surf. Sci.* **2021**, *546*, 149011. [[CrossRef](#)]
17. Gerasimov, G.N.; Gromov, V.F.; Ilegbusi, O.J.; Trakhtenberg, L.I. The Mechanisms of Sensory Phenomena in Binary Metal-Oxide Nanocomposites. *Sens. Actuators B* **2017**, *240*, 613–624. [[CrossRef](#)]
18. Zandi, O.; Agrawal, A.; Shearer, A.; Reimnitz, L.C.; Dahlman, C.J.; Staller, C.M.; Milliron, D. Impacts of Surface Depletion on the Plasmonic Properties of Doped Semiconductor Nanocrystals. *Nat. Mater.* **2017**, *17*, 710–717. [[CrossRef](#)]
19. Ghini, M.; Curreli, N.; Lodi, M.B.; Petrini, N.; Wang, M.; Prato, M.; Fanti, A.; Manna, L.; Kriegel, I. Control of Electronic Band Profiles through Depletion Layer Engineering in Core-Shell Nanocrystals. *Nat. Commun.* **2022**, *13*, 537. [[CrossRef](#)]
20. Kurmangaleev, K.S.; Bodneva, V.L.; Posvyanskii, V.S.; Trakhtenberg, L.I. Sensory Effect toward Hydrogen in a Nanostructured $CeO_2-In_2O_3$ System. *Russ. J. Phys. Chem. A* **2022**, *96*, 2056–2058. [[CrossRef](#)]
21. Madon, M.J.; Morrison, S.R. *Chemical Sensing with Solid State Devices*; Academic Press: San Diego, CA, USA, 1989.
22. Williams, F.A. *Combustion Theory*; CRC Press: Boca Raton, FL, USA, 2018.
23. Wolkenstein, F.F. *Electronic Processes on Semiconductor Surfaces during Chemisorption*; Consultants Bureau, Cop.: London, UK, 1990.
24. Morrison, S.R. *The Chemical Physics of Surfaces*, 2nd ed.; Springer: Dordrecht, The Netherlands, 1990; 456p.
25. Vol'pert, A.I.; Khudyaev, S.I. *Analysis in Classes of Discontinuous Functions and Equations of Mathematical Physics*, 1st ed.; Springer: Dordrecht, The Netherlands, 1985; pp. 626–640.
26. Gelfand, I.M.; Fomin, S.V. *Calculus of Variations*; Prentice-Hall: Hoboken, NJ, USA, 1963.
27. Landau, L.D.; Lifshitz, E.M. *Statistical Physics*; Elsevier Science: Amsterdam, The Netherlands, 1980; Volume 5.
28. Kozhushner, M.A.; Lidskii, B.V.; Oleynik, I.I.; Posvyanskii, V.S.; Trakhtenberg, L.I. Inhomogeneous Charge Distribution in Semiconductor Nanoparticles. *J. Phys. Chem. C* **2015**, *119*, 16286–16292. [[CrossRef](#)]
29. Pines, D. *Elementary Excitations in Solids*; W.A. Benjamin: New York, NY, USA, 1963.
30. Kittel, C. *Introduction to Solid State Physics*, 8th ed.; John Wiley and Sons: New York, NY, USA, 2005.
31. Godunov, S.K.; Ryaben'kii, V.S. *Difference Schemes*; North Holland: Amsterdam, The Netherlands, 1987.
32. Kurmangaleev, K.S.; Trakhtenberg, L.I.; Mikhailova, T.Y. Oxygen Chemisorption on the Surface of an $In_2O_3(011)$ nanocrystal. *Inorg. Mater.* **2020**, *56*, 1138–1146. [[CrossRef](#)]
33. Dixit, A.; Sudakar, C.; Naik, R.; Naik, V.M.; Lawes, G. Undoped Vacuum Annealed In_2O_3 Thin Films as a Transparent Conducting. *Appl. Phys. Lett.* **2009**, *95*, 192105. [[CrossRef](#)]
34. Zuev, D.A.; Lotin, A.A.; Novodvorsky, O.A.; Lebedev, F.V.; Khramova, O.D.; Petuhov, I.A.; Putilin, P.N.; Shatohin, A.N.; Rumyanzeva, M.N.; Gaskov, A.M. Pulsed Laser Deposition of ITO Thin Films and Their Characteristics. *Semiconductors* **2012**, *46*, 410–413. [[CrossRef](#)]
35. Dumesic, J.A.; Milligan, B.A.; Greppi, L.A.; Balse, V.R.; Sarnowski, K.T.; Beall, C.E.; Kataoka, T.; Rudd, D.F.; Trevino, A.A. A Kinetic Modeling Approach to the Design of Catalysts—Formulation of a Catalyst Design Advisory Program. *Ind. Eng. Chem. Res.* **1987**, *26*, 1399–1407. [[CrossRef](#)]
36. Berhanu, T.; Hoffnagle, J.; Rella, C.; Kimhak, D.; Nyfeler, P.; Leuenberger, M. High-Precision Atmospheric Oxygen Measurement Comparisons Between a Newly Built CRDS Analyzer and Existing Measurement Techniques. *Atmos. Meas. Tech.* **2019**, *12*, 6803–6826. [[CrossRef](#)]
37. Varley, J.; Schleife, A. Bethe-Salpeter Calculation of Optical-Absorption Spectra of In_2O_3 and Ga_2O_3 . *Semicond. Sci. Technol.* **2015**, *30*, 024010. [[CrossRef](#)]
38. Trakhtenberg, L.I.; Gerasimov, G.N.; Gromov, V.F.; Belysheva, T.V.; Ilegbusi, O.J. Effect of Composition on Sensing Properties of $SnO_2 + In_2O_3$ Mixed Nanostructured Films. *Sens. Actuators B* **2012**, *169*, 32–38. [[CrossRef](#)]
39. Gerasimov, G.N.; Gromov, V.F.; Ikim, M.I.; Ilegbusi, O.J.; Trakhtenberg, L.I. Effect of Interaction between Components of $In_2O_3-CeO_2$ and SnO_2-CeO_2 Nanocomposites on Structure and Sensing Properties. *Sens. Actuators B* **2019**, *279*, 22–30. [[CrossRef](#)]

Disclaimer/Publisher's Note: The statements, opinions and data contained in all publications are solely those of the individual author(s) and contributor(s) and not of MDPI and/or the editor(s). MDPI and/or the editor(s) disclaim responsibility for any injury to people or property resulting from any ideas, methods, instructions or products referred to in the content.